RSC Advances

ROYAL SOCIETY OF CHEMISTRY

www.rsc.org/advances

A mononuclear diketone-based oxido-vanadium(IV) complex: structure, DNA and BSA binding, molecular docking and anticancer activities against MCF - 7, HPG-2, and HT- 29 cell lines

Maryam Mohamadi [a, b], S.Yousef Ebrahimipour [a,b*] , Masoud Torkzadeh-Mahani [c], Sabine Foro [d], Alireza Akbari [b]

[a] Department of Chemistry, Faculty of Science, Shahid Bahonar University of Kerman, Kerman, Iran

[b] Department of Chemistry, Payam Noor University (PNU), 19395-4697 Tehran, Iran

[c] Department of Biotechnology, Institute of Science, High Technology and Environmental Science, Graduate University of Advance Technology, Kerman, Iran

[d] Materials Science Department, Alarich-Weiss-Str. 2, 64287 Darmstadt, Germany

Corresponding author:

Dr. S. Yousef Ebrahimipour

Department of Chemistry, Shahid Bahonar University of Kerman

76169-14111, Kerman, Iran

Tel/fax: +98 34 3132 2143

E-mails adresses: Ebrahimipour@uk.ac.ir, Ebrahimipour@ymail.com

Abstract

A mononuclear oxido-vanadium(IV) complex, $[VO(L)_2]$, has been prepared from the reaction of dibenzoylmethane (HL) and $VO(acac)_2$ in 2:1 molar ratio, and fully characterized using elemental analyses, molar conductivity, FT-IR, and electronic spectroscopy. The structure of this compound was also confirmed by single crystal X-ray diffraction. It was found that in the title complex, metal coordination geometry is ascribed as distorted square pyramid. DNA binding activities of this complex was investigated using electronic absorption titration, competitive fluorescence titration and cyclic voltametry studies. The obtained results showed groove binding of the complex to the salmon sperm DNA accompanied with a partial insertion of the ligand between the base stacks of the DNA with the binding constant of 2.3×10^3 M^{-1}. In addition, the interaction of the complex with bovine serum albumin (BSA) was studied using electronic absorption and fluorescence spectroscopies at different temperatures indicating a good affinity of the complex for BSA. These experimental results were confirmed by the results of molecular docking. Finally, the in vitro cytotoxicity properties of the synthesized complex against MCF-7, HPG-2 and HT-29 cell lines were evaluated and compared with those of ligand (HL). It was found that complexation improved the anticancer activity significantly. IC_{50} values for the V(IV) complex against MCF-7, HPG-2 and HT-29 cell lines were obtained to be 7.8, 13.5 and 16.1 μM, respectively

Keywords: V(IV) complex, MTT assay , DNA- and BSA binding, Crystal structure, Molecular modeling

Introduction

Vanadium is biocompatible and has a wide variety of biochemical and physiological functions [1] Transition metal complexes containing vanadium(IV) have been shown to modulate the cellular redox potential and catalyze the generation of reactive oxygen intermediates (ROI) resulted in the regulation of enzymatic phosphorylation, and exertion of pleiotrophic effects in multiple biological systems [2-4].

It has been reported that some oxido-vanadium complexes exhibit potent anti-HIV properties [5, 6] Moreover, both inorganic salts and organic chelates of VO^{2+} have been found to be able to participate in glucose uptake and metabolism due to their insulin-mimetic effects [7].

Moreover, since vanadium has the ability to assume various oxidation states, the coordination chemistry of this metal is versatile in biological systems and allows its interaction with different biomolecules [8]. For example, the presence of vanadium species in several proteins including bromoperoxidase and nitrogenase is essential for their catalytic activities [9-11] Or as another example, the insulin-like properties of VO^{2+} chelates has been found to be dependent on the binding of these compounds to BSA and possibly other serum transport proteins [12].

Serum albumin is the most abundant protein in plasma with multiple functions. This protein has the ability to bind reversibly to a large number of compounds so that it is known as the principal carrier of fatty acids, metabolic products, regulatory mediators, and nutrients [13-15].1–5 In addition, serum albumin neutralizes endogenous or exogenous toxins after interaction with them by means of hydrogen bonding [16], hydrophobic, electrostatic, and metal interactions [17].

Vanadium ion was used earlier as an antitumor agent [18]. It has been observed that oxovanadium (IV) complexes show striking similarities to the well-known anticancer drug, *cis*-platin and exhibit anticancer activities [19]. Both V(IV) complexes and *cis*-platin are toxic to cells due to their interactions with nuclear DNA. However, the mechanisms of these interactions are different

from each other. *cis*-platin binds covalently to DNA which makes it a potential mutagen. Unlike *cis*-platin, vanadium complexes interact with nucleotide phosphate groups and do not disturb the Watson-Crick hydrogen bonding [20]. Accordingly vanadium complexes are potential alternatives to platinum-based chemotherapy with limited success due to both intrinsic and acquired drug resistance [21]. The chemistry and biology of vanadium compounds in cancer therapeutics have been recently reviewed by Kioseoglou's group [22].

β-Diketones possess different interesting properties such as antioxidant, anti-leukemia, antimicrobial and anticancer activities [23]. Also, they have hepatoprotective and nephroprotective activities, suppress thrombosis, protect against myocardial infarction and have hypoglycemic and antirheumatic properties [24]. *β*-Diketones have been used as chelating agent to synthesize various metal copmlexes [25].

Generally, molecules which interact with DNA affect DNA replication and transcription and ultimately, induce cell death and apoptosis [26]. So, study of the interaction mode and mechanism of such compounds is of importance which helps us to provide new and even more efficient anticancer drugs. Two broad classes of non-covalent DNA-binding agents have been identified: the intercalators and the groove binders. The intercalators bind by inserting a planar aromatic chromophore between adjacent DNA base pairs, whereas the groove binders fit into the DNA minor groove causing a little perturbation of the DNA Structure [27].

According to the above consideration, we used dibenzoylmethane as chelating agent to synthesize a diketone-base oxido-vanadium(IV) complex. The synthesized complex was fully characterized using spectroscopic and physicochemical methods. Experimental and molecular modeling investigations were also performed to determine the mode and mechanism of the

interaction between the complex and DNA and BSA. Moreover, cytotoxicity of the V(IV) complex against MCF-7, HPG-2 and HT-29 cancerous cell lines were studied using MTT assays.

Results and discussion

A square pyramidal V(IV) complex was prepared by the reaction of dibenzoylmethane and $VO(acac)_2$ in 2:1 molar ratio. The obtained complex was stable in air and soluble in DMSO, DMF and has less solubility in methanol, chloroform and acetonitrile. It was insoluble in *n*-hexane and diethyl ether. Molar conductivity value of title complex was equal to 3.2 ohm^{-1} cm^2 mol^{-1} in DMSO, indicating non-electrolyte behaviors of it. The stability of the complex in PBS buffer was investigated using UV absorption spectroscopy (Fig. S1). No considerable change was observed in the spectrum of the complex during 2 h indicating the stability of $[VO(L)_2]$ in aqueous solution.

Spectral characterization

Assignments of selected prominent IR bands in the 400–4000 cm^{-1} region for $[VO(L)_2]$ are listed in the Experimental section. In the FT-IR spectrum of this compound (Fig. S2), the band with high intensity at 1590 cm^{-1} ascribed to the carbonyl (C=O) vibration [28]. The band appeared at 1480 cm^{-1} is correlated to C=C vibration [29]. The stretching vibration of CO appears at 1318 cm^{-1}. The characteristic band of V=O is located at 994 cm^{-1} [30, 31]. The band with medium intensity appeared at 583 cm^{-1} is assigned to V-O vibrations [32].

The electronic spectra of the title complex were recorded in the DMSO (Fig. S3) and showed two intense peaks at 269 and 368 nm. The first band is attributed to a $\pi \rightarrow \pi^*$ transition of aromatic rings and the latter might arise from ligand to metal charge transfer (LMCT) O(p)→V(d) transitions [33]. Finally, the lower energy absorption band at 659 nm is related to *d-d*

transition. This band is due to $^2B_2 \rightarrow {}^2E$ transition indicating the square pyramidal geometry of an oxido-vanadium(IV) chromophore.

X-ray crystal structure

The ORTEP diagram of $[VO(L)_2]$ is presented in Fig. 1. Also, the selected bond length and angles are listed in Table 1. The X-ray analysis shows that this complex has been crystalized in a monoclinic space group P 21/n with a Z value of 4. In this structure, V(IV) ion is coordinated by oxygen atoms of two monoanionic 1,3-Diphenyl-1,3-propanedionato while, the fifth position is occupied by an oxo group. Five-coordinated complexes may have two main geometries of trigonal bipyramidal (TBP) or square pyramidal (SP). Trigonality index (τ) used for determining the geometry of these compounds, is defined as $(\beta-\alpha)/60$ where β and α are two largest bond angles around the metal center in the coordination environment [34]. In an ideal square pyramid β and α equal to180º and so, τ = 0. While, an ideal trigonal-bipyramidal structure has β=180º and α=120º resulting in τ=1. The trigonality index for the complex synthesized here is calculated to be 0.055 indicating SP geometry for this complex. As can be seen from packing diagram (Fig. S4), the only parameter that stabilizes the lattice structure is van der waals interaction and no hydrogen bond exists in this compound.

Titration of DNA with the complex

The UV spectra of DNA solution recorded upon addition varying concentrations of the complex are given in Fig. 2. A strong absorption band at 259 nm is observed in the spectrum of the DNA corresponding to purine and pyrimidine bases of DNA [35]. It is clear that the intensity of the absorption band of DNA has increased (ca. 62%) with gradual addition of the complex up to

[DNA]/[complex]=0.5. This hyperchromisity is due to the fact that the purine and pyrimidine bases of DNA are exposed because of the binding of the complex to DNA. This observation exhibits that the interaction between the complex and the DNA may have caused a slight change in the conformation of the DNA [36]. So, a DNA intercalating interaction of the complex through the stacking interaction of the aromatic rings of the ligand and the base pairs of DNA is proposed [37]. However, no significant shift is observed in the λ_{max} of the DNA peak which can be due to partial intercalation.

Titration of the complex with DNA

The ligand-based transition at 370 nm was used for the electronic absorption titration with the DNA. Any interaction between the complex and DNA can perturb the intraligand-centered spectral transitions. As seen in Fig. 3, the absorption band of the complex showed a hypochromism of 25.3% upon addition of DNA up to [complex]/[DNA]=0.083 without any significant shift in λ_{max}. Generally, significant hypochromism accompanied by a red shift (bathochromism) is known to be a characteristic of the strong π– π stacking interaction between the aromatic chromophore ligand of a metal complex and the aromatic rings of DNA bases which is called intercalation interaction. Coupling of π orbitals which are also partially filled by electrons reduces the transition probability and thus results in hypochromism [38, 39]. On the other hand, hypochromism that is manifested in terms of a small decline in absorbance and either no or only minor changes in λ_{max} has been correlated to groove binding [40]. Accordingly, it can be suggested that $[VO(L)_2]$ complex interacts with the DNA through the partial insertion of the aromatic rings of the ligand to the DNA duplex and it is also likely that the complex can bind to

the DNA helix via a groove mode [40]. It has been demonstrated that the structure of the complex is one of the most important factors contributing to the DNA binding affinity. However, some factors of ligand including size, geometry, hydrophobicity and hydrogen-bonding ability also influence the overall affinity [41]. As can be seen from Fig. 1, the intercalation of the complex is very difficult because the ligands are not nearly so planar.

Binding constant (K_b) is a useful parameter to evaluate the binding strength of the complex to the DNA and can be determined from the variation in the electronic spectra before and after the addition of DNA by applying Benesi-Hildebrand equation [42, 43] (Eq.1) given below:

$$\frac{A_0}{A - A_0} = \frac{\varepsilon_f}{\varepsilon_b - \varepsilon_f} + \frac{\varepsilon_f}{\varepsilon_b - \varepsilon_f} \frac{1}{K_b[DNA]} \qquad \text{Eq. 1.}$$

Where A_0 is the initial absorbance of free complex, A is the absorbance of the complex in the presence of DNA, ε_f corresponds to the extinction coefficient of the complex in its free form and ε_b refers to the extinction coefficient of the complex in the bound form. The plot of $A_0/(A-A_0)$ versus 1/[DNA] gives a straight line with an intercept of $\varepsilon_f /(\varepsilon_b - \varepsilon_f)$ and a slope of $\varepsilon_f /K_b(\varepsilon_b - \varepsilon_f)$. The value of K_b is calculated from the ratio of the intercept to the slope. According to the results shown in Fig. 3 (inset), K_b for the vanadium complex is calculated to be 2.3×10^3 M^{-1}. This K_b value here is much lower than those reported for classical intercalator (ethidium bromide and [Ru(phen)DPPZ] whose binding constants have been found to be in the order of 10^6–10^7M) [44]. This low affinity may be due to the partial intercalation of the complex and the absence of hydrogen-bonding interactions between the complex and DNA.

Competitive binding experiments in the presence of ethidium bromide

EB, a cationic conjugated planar molecule, is a well-known DNA intercalator. The fluorescence intensity of EB is usually weak. However, it increases upon the interaction with DNA. So, EB is employed as a probe for the spectroscopic study of the interaction between dsDNA and potent intercalating species because of 24-fold decrease in its fluorescence when displaced from an intercalation site [45]. To examine whether the vanadium complex can displace EB from the DNA helix, we have investigated the fluorescence spectra of EB-DNA adduct in the presence of varying amounts of the complex (0-45 μM). The results obtained are shown in Fig. 4. As can be seen, the fluorescence intensity of DNA-EB adduct reduces upon addition of the complexes and this effect increases with increasing the concentration of the complex. This quenching indicates that the complex can drive out EB and take its place in the DNA double helix.

Two control experiments were additionally performed; the emission spectrum of the complex alone, EB alone and EB mixed with the complex at the same ratios as the above experiment. The obtained results depicted in Fig. 4B, showed that the complex had no significant fluorescence contribution in the spectrum of EB. Also, no considerable quenching was observed from the interaction of the complex with non-intercalated EB. Accordingly, the quenching of the fluorescence of EB-DNA system by the complex was due to the interaction of the complex with DNA not EB.

The quenching of EB bound to DNA provoked by the compound is in good agreement (R^2 = 0.786) with the linear Stern–Volmer equation (Eq. 2):

$$\frac{F_0}{F} = 1 + K_{SV}[Q] = 1 + K_q \tau_0 [Q] \qquad \text{Eq. 2.}$$

where F_0 and F are the fluorescence intensities in the absence and presence of the quencher or complex (Q), respectively. K_q is the bimolecular quenching constant and τ_0 is the lifetime of the

fluorophore in the absence of the quencher. Stern–Volmer constant (K_{SV}) can be obtained from the slope of the plot of F_0/F versus [Q] with forcing the intercept to 1 (Fig. 4A, insets). Accordingly, the value of K_{SV} for the complex is 2.1×10^3 M^{-1}. K_q was calculated as 2.1×10^{11}.

Electrochemical characterization of the interaction between DNA and the complex

The interaction of the complex with DNA has been also investigated by monitoring the changes observed in the cyclic voltammogram of the complex in 0.02 M PBS upon addition of the DNA. The obtained results are depicted in Fig. 5. The cyclic voltammogram of the complex exhibits a quasi-reversible single electron redox process assignable to the V(VI)/V(V) couple. $[VO(L)_2]$ is oxidized to the mono cation $[VO(L)_2]^+$ [46]. The electron is removed from nonbonding orbitals and the V(V) complex is formed. Upon reversal of the scan direction, the V(V) complex is reduced to V(IV) [47] .

The cathodic and anodic peak potentials appear at E_{pc} = +0.40 V and E_{pa} = +0.32 V with I_{pc} = -7.8 µA and I_{pa} =4.2 µA, respectively. Also, CV of 60 µM DNA in PBS was recorded at the same conditions. As seen, no peak was observed in the scanned potential range. In the presence of 60 µM DNA, E_{pc} shifted to +0.45 V while E_{pa} showed no considerable change. Also, both the cathodic and anodic peak currents decreased to -6.1 µA and +1.8 µA, respectively due to the reduced diffusion rate of the complex towards the electrode surface as a result of the interaction with the bulky, slowly diffusing DNA.

Peak separation (ΔE_p) and half-wave potential ($E^0_{1/2}$) are defined as the difference and the average of E_{pa} and E_{pc}, respectively. Using the changes made in the values of ΔE_p and $E^0_{1/2}$ after addition of DNA, one can explain the ability of the interaction. It was observed that addition of

the DNA increased ΔE_p from 0.08 to 0.13 V and $E^0_{1/2}$ from 0.36 V to 0.385 V. It has been reported that an intercalative binding mode between molecules and DNA causes a positive shift in the half-wave potential while an electrostatic binding mode results in a negative shift [48]. According to the results obtained, the increase of the formal potentials of the complexes accompanied by the decrease of the peak currents observed in the presence of the DNA suggests that the complex has interacted with the DNA in an intercalative mode.

BSA interaction

UV–Vis absorption studies

Binding to BSA involved in the transport of the complex through the blood stream may result in lower or enhanced biological properties of the original drug, or new paths for the drug transportation. [49] Absorption titration was used to examine the conformational change of BSA after complex formation with $[VO(L)_2]$. Fig. 6 shows the absorption spectra of BSA in the presence of varying concentrations of the complex. In the spectrum of BSA, the absorption peak at 279.9 nm originates from the phenyl rings in aromatic acid residues (Trp, Tyr and Phe) [50]. Upon addition of the complex, the intensity of the peak increased sharply with a blue shift of 4 nm, suggesting an interaction between BSA and the title V(IV) complex and also change of the polarity of the microenvironment surrounded the aromatic amino acid residues of BSA [51].This can be put down to the exposure of the aromatic amino acid residues originally buried in a hydrophobic cavity, to an aqueous milieu. This exposure is happened after π– π stacking interaction between aromatic ring of the complex and those of the aromatic amino acid residues [52].

Fluorescence quenching studies

The protein binding of the complex was studied using tryptophan fluorescence quenching experiments for BSA as the substrate in PBS (pH 7.0). Binding of the complex to BSA results in some conformational changes of the protein. These changes influence the fluorescence emission of tryptophan residues [53]. Therefore, the fluorescence spectra of tryptophan residues of BSA in the range of 300–470 nm (excited at 276 nm) were monitored using increasing concentrations of the complex as quencher. Interaction between the complex and BSA resulted in the quenching of the fluorescence of BSA. Fig. 7. (A, B and C) shows the fluorescence spectra of BSA in the absence and presence of different amounts of the complex at 291, 298 and 305 K, respectively. In all three temperatures, the extent of the quenching increases with increasing the concentration of the complex.

The possible quenching mechanism can be interpreted using Eq. 2 [54]. Taking the fluorescence lifetime (τ_0) of tryptophan at 10^{-8} s, the approximate quenching constant (K_q) of the complex is calculated. Fig. S5 reveals the plots of F_0/F vs. the concentration of the complex, [Q] at different temperatures. The values of K_{SV} and K_q obtained from the ratio of the slope to the intercept of the plot are given in Table 2. The values of K_{SV} are of 4 magnitude order indicating a moderate quenching.

Binding constants and binding sites

If it is assumed that there are similar and independent binding sites in the biomolecule, the binding constant (K_b) and the number of the binding sites (n) can be determined using the slope and intercept of the double logarithm regression curve of log [(F_0 F)/F] versus log [Q] based on Lineweavere-Burk equation (Eq. 3) [55]:

$$\log\frac{F_0 - F}{F} = \log K_b + n\log[Q] \quad \text{Eq. 3.}$$

where F_0 and F are the fluorescence intensities of BSA in the absence and presence of the complex (Q), respectively. K_b is the binding constant of the complex to BSA and n is the number of binding sites per albumin molecule. Fig. 8 reveals the plots of $\log\frac{F_0-F}{F}$ versus log[Q] for the binding of V(IV) complex to BSA at different temperatures. From the intercept and slope of the plot, K_b and n values can be calculated. The values of K_b and n obtained for BSA–V(IV) Complex adduct are given in Table 2. As seen, K_b value decreases with increasing temperature indicating the binding process is exothermic [53, 56].

In general, the binding constant of a compound to a protein such as albumin should be high enough to allow transfer by the protein and on the other hand, not too high so that it can be released upon arrival at its target(s). A strong interaction between protein and a typical complex has been reported to have a binding constant ranging from 10^6 to 10^8 M^{-1} [57]. Accordingly, the values of K_b obtained here for BSA-$[VO(L)_2]$ system are considered a moderate binding affinity. The value of n is nearly 1 at 298 and 291 K suggesting that the complex bond to BSA according to the molar ratio of 1:1. But at 305 K, n value decreases which is consistent to the exothermic nature of the interaction.

Thermodynamic parameters and binding mode

The sign and magnitude of thermodynamic parameters enthalpy change (ΔH), entropy change (ΔS) and free energy change (ΔG) are useful to determine the binding mode. It has been found that, $\Delta H > 0$ and $\Delta S > 0$ arise from a hydrophobic interaction, $\Delta H < 0$ and $\Delta S < 0$ arise from a

van der Waals force or hydrogen bond formation, while $\Delta H \approx 0$ and $\Delta S > 0$ arise from an electrostatic force [58].

The values of ΔH and ΔS can be obtained from the van't Hoff equation(Eq. 4):

$$logK_b = -\frac{\Delta H}{2.303RT} + \frac{\Delta S}{2.303R} \quad \text{Eq. 4.}$$

where K_b is the binding constant, T is the absolute temperature and R is the gas constant. ΔH and ΔS values are obtained by plotting the values of $logK_b$ vs. 1/T.

Fig. S6 shows the van't Hoff plot for the V(IV) complex-BSA system which is a straight line. From the slope and intercept of this plot, ΔH and ΔS are calculated, respectively which are given in Table 3. In addition, the values of ΔG at different temperatures calculated according to Eq 5. are shown in Table 3.

$\Delta G = \Delta H - T\Delta S$ Eq 5.

The negative values of ΔG reveal that the binding process is spontaneous and also the values of ΔH with negative signs are much greater than TΔS values indicating that BSA-V(IV) complex formation is mainly enthalpy-driven reaction. Moreover, both negative ΔH and ΔS values indicate that van der Waals force or hydrogen bond interaction plays major role in the interaction between BSA and the complex.

Molecular docking of the V(IV) complex with DNA

Binding sites involving in the interaction between the complex and DNA was determined using blind docking on a double-stranded DNA (strands A and B shown in Fig. 9) with the following sequence:

A: 5'(C11, G22, C33, G44, A55, A66, T77, T88, C99, G110, C11, G112) 3'

B: 3' (G224, C223, G222, C221, T220, T119, A118, A117, G116, C115, G114, C113) 5'

The grid map set to 50×54×116 $Å^3$ along the x, y, and z axes with 0.375 Å grid spacing. The conformations obtained were ranked based on the lowest free binding energy. According to the most stable docking conformation (Fig.9), the V(IV) complex inserted into the minor groove of the DNA duplex with a partial intercalation. As Fig.9 indicates, several categories of hydrophobic contacts are observed between the complex atoms and the bases of DNA, including, Guanine 224, Cytosine 223, Guanine 222 and Cytosine 221 (chain B), Adenine 66, Adenine 55 and Guanine 44 in chain A. The resulting relative binding energy for the complex docked with DNA was found to be -4.48 kcal mol^{-1}.

Molecular docking of the V(IV) complex with BSA

Investigating the interaction of the V(IV) complex with BSA using blind docking showed that the complex prefers the binding pocket of domain II. The resulting conformations were ranked based on their lowest free binding energies. The docking studies showed that this complex interacts with BSA via hydrophobic contacts to amino acid residuals (Fig. 10). Hydrophobic interactions were observed between O1, O3, O5, C3-C16, C18, C21, and C23-C28 of the V (IV) complex with Leu 454, Leu 189, Leu 112, Ile 455, Ala 193, Arg 458, Arg 196, Arg 144, Arg 427, Ser192, Ser 109, Ser 428, Asp 108, Asp 111, pro 146, Asp 110, His 145 and Glu 424. The resulting relative binding energy for the complex docked with BSA was found to be -7.58 kcal mol^{1}.

Cytotoxicity Study

The ligand and complex have been tested for their in-vitro anti-proliferative activity against HPG-2, HT-29 and MCF-7 cancer cell lines. The plot of the percentage of cell viability vs. concentration of the compound is shown in Fig.11. As seen, the viability of all cell lines

decreases in both ligand- and complex-treated ones as a function of concentration indicating a dose-dependent growth inhibitory effect. It is clear that the toxicity of the V(IV) complex against MCF-7 is significantly higher than that of the ligand (HL). In all tested concentrations, the free ligand (HL) showed less than 50% of the toxicity of $[VO(L)_2]$ indicating an enhancement in the anticancer property of the ligand duo to complexation and presence of the vanadium ion. As reported previously, the biological activity of a ligand is usually amplified after complexation [29]. Similarly against HPG-2, the complex is much more toxic than the free ligand especially at lower concentrations. Surprisingly, no preference is observed between the activity of the ligand and the complex against HT-29. This indicates that the sensitivity of HT-29 cells to the ligand is similar to the complex. Moreover, at the concentrations of 0.31, 0.62, 1.25 and 2.5 μM the viability of HPG-2 cells is influenced by the complex more than two other cell lines. While, at higher concentrations of the complex this is MCF-7 which shows the lowest viability. It is worth mentioning that, the side effect of the compound at high concentrations should be also considered.

Furthermore, IC_{50} values for the complex against MCF-7, HPG-2 and HT-29 cell lines were calculated to be 7.8, 13.5 and 16.1 μM, respectively which are smaller than those reported for the well-known anticancer drug, *cis*-platin (22.8, 16.7 and 69.4 μM , respectively) [59] and smaller than or comparable with other vanadium complexes (>50 μM against MCF-7 for VO(sal-Gly)(bipy), VO(sal-Gly)(phen), VO(sal-L-Phe)(H2O), VO(sal-L-Phe)(bipy) and VO(sal-L-Phe)(phen) [60], >47 μM against HT-29 for [VO(sal-L-tryp)(acetylethTSC)] $\cdot C_2H_5OH$, [VO(sal-L-tryp)(MeATSC)] and [VO(salL-tryp)(N-ethhymethohcarbthio)] $\cdot H_2O$ [59b] and 1486 $\mu g/cm^3$ against HPG-2 for V(2-[(4 morpholinophenyl imino) methyl] phenol)$_2$ [61]. However, some more

effective vanadium complexes have been previously synthesized. For example, bis(4, 7-dimethyl-1, 10- phenanthroline) sulfatooxovanadium (IV) with IC_{50} values smaller than 1 μM [62].

Experimental

Materials and Methods

Salmon sperm DNA was purchased from Sigma (St. Louis, USA). A 1.0 mg/mL stock solution of the DNA was prepared in TE buffer (pH 7.4) and kept frozen. The concentration of the solution was determined using the molar extinction coefficient of DNA bases at 260 nm (ε_{260}) which was found to be 6600 L mol^{-1} cm^{-1} (per P or nucleotide unit). Ethidium bromide (EB=3,8-diamino-5-ethyl-6-phenylphenanthridinium bromide) was purchased from CinnaGen (Iran). Bovine serum albumin (BSA) was obtained from Merck (Germany). 3-(4,5-dimethyl-2-thiozolyl)-2,5-diphenyl-2H-tetrazolium bromide (MTT) was purchased from Sigma.

Instrumentation

Elemental analyses were carried out using a Thermo Finnigan Flash Elemental Analyzer 1112EA. FT-IR spectra were recorded at a Bruker-Tensor 27 by embedding the material in KBr discs in the range of 400-4000 cm^{-1}. Molar Conductance measurements were made by means of a Metrohm 712 Conductometer in DMSO. Cyclic voltammograms were obtained using an Autolab PGSTAT 302 electrochemical system from Metrohm (Herisau, Switzerland) interfaced with a personal computer for data acquisition and potential control. Electronic spectra were recorded on a double beam UV-vis-NIR Varian Cary 500 spectrophotometer (Victoria, Australia). Fluorescence measurements were performed on a Cary Eclipse fluorescence spectrophotometer.

Synthesis of bis(1,3-Diphenyl-1,3-propanedionato)-oxido-vanadium(IV) [$VO(L)_2$]

A mixture of dibenzoylmethane (0.045 g, 0.2 mmol) and $VO(acac)_2$ (0.03 g, 0.1 mmol) was refluxed in 10 ml ethanol. After 1 h, the resulted deep green precipitate was filtered, washed with cold ethanol and dried in vacuum over anhydrous $CaCl_2$. Suitable crystals for X-ray crystallography were obtained after slow evaporation of the mother liquor for 1 day at room temperature.

Yield: 0.04 g, 78%. m.p.: 201 °C. Molar conductance (1×10^{-3} M, DMSO): 3.2 ohm^{-1} cm^2 mol^{-1}. Anal. Calc. for $C_{30}H_{22}O_5V$ (513.43 g mol^{-1}): C, 70.18; H, 4.32; N, 15.58. Found: C, 70.03; H, 4.25; N, 15.43% FT-IR (KBr), cm^{-1}: ν(CH_{ar}) 2842-3057, ν(C=O) 1590, ν($C=C_{ring}$) 1480, ν(C-O) 1318, ν(V=O) 994, ν(V-O) 583. UV/Vis (DMSO), λ_{max}, nm (log(ε), L mol^{-1} cm^{-1}): 269(4.49), 368(4.52), 659(3.12).

Crystal structure determination

X-ray diffraction data were collected using an XCalibur diffractometer, Oxford Diffraction Ltd., with sapphire CCD detector in ω-scan mode. Graphite monochromated Mo Ka radiation (λ= 0.71013 Å) has been used. The structure was solved using direct methods with SHELXS-97 and refined on F^2 with full-matrix least squares using SHELXS-97 [63]. The H atoms were positioned with idealized geometry using a riding model with the aromatic C-H distance restrained to 0.93 Å and were refined with isotropic displacement parameters set at 1.2 U_{eq} (C-aromatic) of the parent atom. The crystallographic data for X-ray analysis of title complex is gathered in Table 4.

DNA binding studies

UV-Vis absorption studies

The interaction of the title complex with DNA has been studied by UV spectroscopy in order to investigate the possible binding mode and to calculate the binding constant (K_b). Absorption titration of DNA with the complex was carried out using fixed concentration of DNA (5.8×10^{-4} M) in 0.02 M PBS (pH=7.4) while the concentration of the complex was gradually increased. In the absorption titration of the complex with DNA, the UV-Vis spectra of the complex (4.5×10^{-5} M in PBS) in the presence of varying concentrations of DNA were recorded [64]. It is worthy of note that an appropriate blank sample containing the corresponding concentrations of DNA/complex was used prior to each measurement.

All experiments were carried out at room temperature. In all experiments, the incubation time for the DNA and the complexes to equilibrate was 5 min.

Competitive fluorescence study with DNA-EB adduct

Competitive studies of the $[VO(L)_2]$ compound with EB study was investigated by fluorescence emission spectroscopy in order to examine whether it is able to displace EB from DNA–EB adduct. In this study, a 0.02 M PBS solution (pH=7.4) containing 1.0×10^{-5} M EB and 7.5×10^{-5} M DNA was titrated with the complex. During the fluorescence quenching experiment, emission spectra of DNA-EB adduct were recorded in the range of 535–700 nm upon excitation at 525 nm.

Cyclic voltammetric measurements

Electrochemical techniques can be employed to study the interaction of electro-active complexes with DNA in order to confirm the binding mode suggested by the spectroscopic studies. Cyclic

voltammograms of the V(IV) complex were recorded before and after the addition of DNA to a fixed concentration of the complex in 0.02 M PBS at the scan rate of 100 mV/s.

BSA binding studies

UV-Vis absorption studies

Absorption titration experiment was performed by keeping the BSA concentration constant (2×10^{-5} M) and varying that of the oxido-vanadium(IV) complex (0- 4×10^{-5} M). The absorption spectra of BSA were recorded after each successive addition of the complex and 10 min equilibration. Also, appropriate blank samples containing the corresponding concentrations of BSA/complex were used prior to all measurements.

Fluorescence studies

BSA possesses a strong fluorescence emission due to its aromatic amino acids (Trp, Tyr, and Phe). However, the intrinsic fluorescence intensity of BSA when excited at 290 nm mainly comes from the tryptophan residues [65, 66]. A fluorescence quenching study was performed to investigate the interaction between BSA and $[VO(L)_2]$. In this study, a fixed concentration of BSA (7.5×10^{-5} M in 0.02 M PBS), was titrated by successive additions of the complex. The mixture was allowed to equilibrate for 5 min after each addition. The fluorescence spectra were obtained from 300 nm to 470 nm using the excitation wavelength of 290 nm at different temperatures.

Cell Proliferation and viability assay

Toxicity of $[VO(L)_2]$ and ligand (HL) against three human carcinoma cell lines namely HPG-2, HT-29 and MCF-7 was investigated using MTT assay. MTT is transformed into formazan by

the enzyme hydrogenase in mitochondria. The surviving cells can be determined by measuring their ability to reduce MTT (yellow) to formazan product (purple). Cytotoxicity of the compound against each cell line was then concluded from dose–response curves.

The cells were placed in 96-well micro-assay culture plates at a density of 5×10^3 cells per well and grown at 37 ˚C in a humidified 5% CO_2 incubator for 24 h. Then the cells were treated with varying concentrations (0.31, 0.62, 1.25, 2.5, 5, 10, 20 and 40 μM) of the complex and ligand for 24 h. After that, 20 μl of MTT solution was added to each plate and incubation was performed at 37 ˚C for 4 h. The metabolically active cells reduced MTT to blue formazan crystals. The crystals formed were then solubilized upon addition of DMSO and incubated at room temperature for 20 min. Finally, the absorbance (A) of the solution of each well was measured with ELISA reader at 545 nm. The absorbance was converted to percentage of cell growth inhibition according to the following formula:

$$\%\text{Cell cytotoxicity} = [1 - (A_{drug}/A_{control})] \times 100$$

The values of IC_{50} defined as the concentrations of test compound required to reduce the survival of cells by 50%, were also calculated.

Molecular docking

Molecular docking is a powerful method to predict the orientation of a ligand when binds to a receptor. Herein, the intermolecular interaction of the V(IV) complex with DNA and BSA were investigated using molecular docking. The coordination sphere of the V(IV) complex was generated from its X-ray crystal structure as a CIF file. Then, the CIF file was converted to the PDB format using Mercury software (http://www.ccdc.cam.ac.uk/). Molecular docking study was performed with Autodock 4.2.6 software using the implemented empirical free energy

function and the Lamarckian Genetic Algorithm [67]. The structures of the receptors were kept rigid during the docking while the metal complex was allowed to have rotatable bonds. Discovery Studio Visualizer 4.1 package (Accelrys Inc., San Diego, CA) was used for the production of molecular images and animations. The schematic two-dimensional representations of the docking results were performed using LIGPLOT+ [68].

Chemical structures of DNA and BSA

The initial structure of BSA with the PDB ID of 4F5S was taken from Protein Data Bank at a resolution of 2.47 Å. Also, a DNA with the sequence of $d(CGCGAATTCGCG)_2$ was obtained from the Protein Data Bank (PDB ID: 1BNA) at a resolution of 1.90 Å.

Conclusions

An oxido-vanadium(IV) complex $[VO(L)_2]$, containing dibenzoylmethane ligand has been synthesized and fully characterized using various physicochemical and spectroscopic methods including single crystal X-ray diffraction. The central vanadium(IV) ion is situated in a distorted square pyramidal environment (O_5 chromophore). The square plane is made up of donor oxygen atoms of 1,3-Diphenyl-1,3-propanedionato (L^-). The oxido group occupies the axial position. DNA binding activities of this complex have been investigated with electronic absorption, competitive fluorescence titration and cyclic voltammetry techniques. The obtained results have suggested a groove binding mode of interaction accompanied with a partial intercalation into the DNA helix with the DNA-binding constant in order of 10^3 M^{-1}. Study of the interaction between the title complex and BSA indicates a good binding propensity to BSA. So, this protein can be a suitable carrier for the complex. The results of molecular docking reveal that the complex fits

into the minor groove of DNA along with partial intercalation and prefers the binding pocket in domain II of BSA which are in good agreement with those of experimental studies. Anticancer activities of $[VO(L)_2]$ against three carcinoma cell lines of MCF-7, HPG-2 and HT-29 have been investigated using MTT assay. The values of IC_{50} (7.8, 13.5 and 16.1 μM for MCF-7, HPG-2 and HT-29, respectively) indicate that $[VO(L)_2]$ synthesized here, can be proposed as an efficient metal-based anticancer drug. However, further considerations including in vivo studies should be performed to fully evaluate the cell toxicity of the synthesized complex.

Supplementary materials

Crystallographic data for the $[VO(L)_2]$ has been deposited with the Cambridge Crystallographic Data Centre, CCDC No. 1034152. Copies of this information may be obtained from the Director, CCDC, 12 Union Road, Cambridge, CB2 1EZ, UK (fax: +44-1223-336033; e-mail: deposit@ccdc.cam.ac.uk or http://www.ccdc.cam.ac.uk).

Acknowledgment

We are grateful to Shahid Bahonar University of Kerman for financial support and Prof. W. Haase for helping us to determine X-ray crystal structure of the synthesized complex.

References

1. H. Michibata, *Vanadium: Biochemical and Molecular Biological Approaches*, Springer Netherlands, 2011.
2. J. Z. Byczkowski, B. Wan and A. P. Kulkarni, *Bull. Environ. Contam. Toxicol.*, 1988, **41**, 696-703.
3. O. J. D'Cruz, P. Ghosh and F. M. Uckun, *Mol. Hum. Reprod.*, 1998, **4**, 683-693.
4. X. Shi, P. Wang, H. Jiang, Y. Mao, N. Ahmed and N. Dalal, *Ann. Clin. Lab. Sci.*, 1996, **26**, 39-49.
5. O. J. D'Cruz, Y. Dong and F. M. Uckun, *Biochem. Biophys. Res. Commun.*, 2003, **302**, 253-264.
6. S. Shigeta, S. Mori, E. Kodama, J. Kodama, K. Takahashi and T. Yamase, *Antivir. Res.*, 2003, **58**, 265-271.
7. D. Rehder, *Dalton Trans.*, 2013, **42**, 11749-11761.
8. E. G. Ferrer, A. Bosch, O. Yantorno and E. J. Baran, *Biorg. Med. Chem.*, 2008, **16**, 3878-3886.
9. D. C. Crans, J. J. Smee, E. Gaidamauskas and L. Yang, *Chem. Rev.*, 2004, **104**, 849-902.
10. C. Leblanc, H. Vilter, J.-B. Fournier, L. Delage, P. Potin, E. Rebuffet, G. Michel, P. Solari, M. Feiters and M. Czjzek, *Coord. Chem. Rev.*, 2015.
11. Y. Hu and M. W. Ribbe, *J. Biol. Inorg. Chem.*, 2015, **20**, 435-445.
12. M. W. Makinen and M. J. Brady, *J. Biol. Chem.*, 2002, **277**, 12215-12220.
13. M. Nonaka, E. Li-Chan and S. Nakai, *J. Agric. Food. Chem.*, 1993, **41**, 1176-1181.
14. M. M. Yamashita, L. Wesson, G. Eisenman and D. Eisenberg, *Proc. Natl. Acad. Sci.*, 1990, **87**, 5648-5652.
15. W. Bal, J. Christodoulou, P. J. Sadler and A. Tucker, *J. Inorg. Biochem.*, 1998, **70**, 33-39.
16. H. M. Rawel, S. Rohn, H.-P. Kruse and J. Kroll, *Food Chem.*, 2002, **78**, 443-455.
17. Y. Zhang and D. E. Wilcox, *J. Biol. Inorg. Chem.*, 2002, **7**, 327-337.
18. a) A. M. Evangelou, *Crit. Rev. Oncol. Hematol.*, 2002, **42**, 249-265; b) D. C. Crans, L. Yang, J. A. Alfano, L.-H. Chi, W. Jin, M. Mahroof-Tahir, K. Robbins, M. M. Toloue, L. K. Chan and A. J. Plante, *Coord. Chem. Rev.*, 2003, **237**, 13-22.

19. a) P. Ghosh, O. J. D'Cruz, R. K. Narla and F. M. Uckun, *Clin. Cancer Res.*, 2000, **6**, 1536-1545; b) O. J. D'Cruz, Y. Dong and F. M. Uckun, *Anti-cancer drugs*, 2000, **11**, 849-858.
20. M. M. Harding and G. Mokdsi, *Curr. Med. Chem.*, 2000, **7**, 1289-1303.
21. a) L. R. Kelland, *Drugs*, 2000, **59**, 1-8; b) G. Giaccone, *Drugs*, 2000, **59**, 9-17.
22. E. Kioseoglou, S. Petanidis, C. Gabriel and A. Salifoglou, *Coord. Chem. Rev.*, 2015, in press. doi:10.1016/j.ccr.2015.03.010
23. a) W. Urbaniak, K. Jurek, K. Witt, A. Goraczko, *CHEMIK,* 2011, **65(4)**, 273-282; b) M. T. Huang,Y. R. Lou, J. G. Xie,W. Ma, Y. P. Lu, P. Yen, B. T. Zhu, H. Newmark and C. T. Ho, *Carcinogenesis*, 1998, **19(9)**, 1697-1700; c) J. R. Dimmock, S. K. Raghavan and G. E. Bigam, *Eur. J. Med. Chem*, 1988, **23(2)**, 111-117; d) J. Sheikha, A. Parvez, H. Juneja, V. Ingle, Z. Chohan, M. Youssoufi and T. B. Hadda, *Eur. J. Med. Chem*, 2011, **46(4)**, 1390-1399; e) P. Anand, S. G. Thomas, A. B. Kunnumakkar, C. Sundaram, K. B. Harikumar, B. Sung, S. T. Tharakan, K. Misra, I. K. Priyadarsini, K. N. Rajasekharan, B. B. Aggarwal, *Biochem. Pharmacol*., 2008, **76**, 1590–1611.
24. P. Anand, S. G. Thomas, A. B. Kunnumakkara, C. Sundaram, K. B. Harikumar, B. Sung, S. T. Tharakan, K. Misra, I. K. Priyadarsini, K. N. Rajasekharan, B. B. Aggarwal, *Biochem. Pharmacol*., 2008 **76(11)**, 1590-611.
25 P. A. Vigato, V. Peruzzo and S. Tamburini, *Coord. Chem. Rev*., 2009, **253**, 1099-1201
26. W. P. Roos and B. Kaina, *Trends Mol. Med.*, 2006, **12**, 440-450.
27. J. B. Chaires, *Curr. Opin. Struct. Biol.*, 1998, **8**, 314-320.
28. a) S. Y. Ebrahimipour, I. Sheikhshoaie, A. Crochet, M. Khaleghi and K. M. Fromm, *J. Mol. Struct.*, 2014, **1072**, 267-276; b) S. Y. Ebrahimipour, I. Sheikhshoaie, M. Mohamadi, S. Suarez, R. Baggio, M. Khaleghi, M. Torkzadeh-Mahani and A. Mostafavi, *Spectrochim. Acta, Part A*, 2015, **142**, 410-422.
29. S. Y. Ebrahimipour, I. Sheikhshoaie, J. Castro, W. Haase, M. Mohamadi, S. Foro, M. Sheikhshoaie and S. Esmaeili-Mahani, *Inorg. Chim. Acta*, 2015, **430**, 245-252.
30. S. Y. Ebrahimipour, I. Sheikhshoaie, A. C. Kautz, M. Ameri, H. Pasban-Aliabadi, H. A. Rudbari, G. Bruno and C. Janiak, *Polyhedron*, 2015, **93**, 99-105.

31. S. Y. Ebrahimipour, M. Abaszadeh, J. Castro and M. Seifi, *Polyhedron*, 2014, **79**, 138-150.
32. I. Sheikhshoaie, S. Y. Ebrahimipour, A. Crochet and K. M. Fromm, *Res. Chem. Intermed.*, 2015, **41(4)**, 1881-1891.
33. S. Y. Ebrahimipour, J. T. Mague, A. Akbari and R. Takjoo, *J. Mol. Struct.*, 2012, **1028**, 148-155.
34. A. W. Addison, T. N. Rao, J. Reedijk, J. van Rijn and G. C. Verschoor, *J. Chem. Soc., Dalton Trans.*, 1984, 1349-1356.
35. K. C. Skyrianou, V. Psycharis, C. P. Raptopoulou, D. P. Kessissoglou and G. Psomas, *J. Inorg. Biochem.*, 2011, **105**, 63-74.
36. J.-Q. Sha, X. Li, H.-B. Qiu, Y.-H. Zhang and H. Yan, *Inorg. Chim. Acta*, 2012, **383**, 178-184.
37. A. Silvestri, G. Barone, G. Ruisi, D. Anselmo, S. Riela and V. T. Liveri, *J. Inorg. Biochem.*, 2007, **101**, 841-848.
38. R. Fiel, J. Howard, E. Mark and N. D. Gupta, *Nucleic Acids Res.*, 1979, **6**, 3093-3118.
39. A. Terenzi, G. Barone, A. Silvestri, A. M. Giuliani, A. Ruggirello and V. T. Liveri, *J. Inorg. Biochem.*, 2009, **103**, 1-9.
40. a) F. Darabi, H. Hadadzadeh, M. Ebrahimi, T. Khayamian and H. A. Rudbari, *Inorg. Chim. Acta*, 2014, **409**, 379-389; b) P.-x. Xi, Z.-h. Xu, X.-h. Liu, F.-j. Cheng and Z.-z. Zeng, *Spectrochim. Acta, Part A*, 2008, **71**, 523-528
41. A. M. Pyle, J. P. Rehmann, R. Meshoyrer, C.V. Kumar, N. J. Turro and J. K. Barton, *J. Am. Chem. Soc.,* 1989, **111**, 3051–3058.
42. I. Kuntz Jr, F. Gasparro, M. Johnston Jr and R. Taylor, *J. Am. Chem. Soc.*, 1968, **90**, 4778-4781.
43. R. L. Scott, *Recl. Trav. Chim. Pays-Bas*, 1956, **75**, 787-789.
44 a) M. Cory, D. D. McKee, J. Kagan, D. W. Henry and J. A. Miller, *J. Am. Chem. Soc*., 1985, **107**, 2528–2536; b) M. J. Waring, *J. Mol. Biol*., 1965, **13**, 269–282; c) V. G. Vaidyanathan and B. U. Nair, *J. Inorg. Biochem*., 2003, **94**, 121–126; d) R. Vijayalakshmi, M. Kanthimathi, V. Subramanian and B.U. Nair, *Biochim. Biophys. Acta,* 2000 **1475**, 157–162

45. D. Suh and J. B. Chaires, *Biorg. Med. Chem.*, 1995, **3**, 723-728.

46. A. H. Kianfar and S. Mohebbi, *J. Iranian Chem. Soc*., 2007, **4,** 215–220.48

47. A. H. Kianfar, M. Paliz, M. Roushani and M. Shamsipur, *Spectrochim. Acta A*, 2011, **82(1),** 44-48.

48. M. T. Carter, M. Rodriguez and A. J. Bard, *J. Am. Chem. Soc*. 1989, **111**, 8901–8911

49. P. Tsilikia, F. Perdihb, I. Turelb and G. Psomas, *Polyhedron*, 2013, **53**, 215-222.

50. Y. Wang, X. Wang, J. Wang, Y. Zhao, W. He and Z. Guo, *Inorg. Chem.*, 2011, **50**, 12661-12668.

51. G. Zhang, Y. Ma, L. Wang, Y. Zhang and J. Zhou, *Food Chem.*, 2012, **133**, 264-270.

52. X.-B. Fu, Z.-H. Lin, H.-F. Liu and X.-Y. Le, *Spectrochim. Acta, Part A*, 2014, **122**, 22-33.

53. M. Anjomshoa, H. Hadadzadeh, M. Torkzadeh-Mahani, S. J.Fatemi, M. Adeli-Sardou, H. Amiri Rudbarid and V. M. Nardoe, *Eur. J. Med. Chem.*, 2015, **96**, 66-82.

54. A. Castiñeiras, N. Fernández-Hermida, I. García-Santos and L. Gómez-Rodríguez, *Dalton Trans.*, 2012, **41**, 13486-13495.

55 a) M. Jiang, M. X. Xie, D. Zheng, Y. Liu, X. Y. Li, X. Chen, *J. Mol. Struct*. 2004, **692**, 71-80; b) V. Anbazhagan and R. Renganathan, *J. Lumin*. 2008, **128**, 1454-1458.

56. B. Ahmad, S. Parveen and R. H. Khan, *Biomacromolecules*, 2006, **7**, 1350-1356.

57. a) J. Zhang, X.-J. Wang, Y.-J. Yan and W.-S. Xiang, *J. Agric. Food. Chem.*, 2011, **59**, 7506-7513; b) J. Xiao, M. Suzuki, X. Jiang, X. Chen, K. Yamamoto, F. Ren and M. Xu, *J. Agric. Food. Chem.*, 2008, **56**, 2350-2356; c) J. Liu, J. Tian, Z. Hu and X. Chen, *Biopolymers*, 2004, **73**, 443-450; d) N. A. Kratochwil, W. Huber, F. Müller, M. Kansy and P. R. Gerber, *Biochem. Pharmacol.*, 2002, **64**, 1355-1374; e) P. Bourassa, S. Dubeau, G. M. Maharvi, A. H. Fauq, T. Thomas and H. Tajmir-Riahi, *Eur. J. Med. Chem.*, 2011, **46**, 4344-4353

58. P. D. Ross and S. Subramanian, *Biochemistry*, 1981, **20**, 3096-3102.

59. a) Y. Chen, M.-Y. Qin, J.-H. Wu, L. Wang, H. Chao, L.-N. Ji and A.-L. Xu, *Eur. J. Med. Chem.*, 2013, **70**, 120-129; b) N. A. Lewis, F. Liu, L. Seymour, A. Magnusen, T. R. Erves, J. F. Arca, F. A. Beckford, R. Venkatraman, A. G. Sarrías, F. R. Fronczek, D. G. VanDerveer, N. P. Seeram, A. Liu, W. L. Jarrett and A. A. Holder, *Eur. J. Inorg. Chem*., 2012, **2012(4)**, 664-677

60 I. Correia, S. Roy, C. P. Matos, S. Borovic, N. Butenko, I. Cavaco, F. Marques, J. Lorenzo, A. Rodríguez, V. Moreno and J. C. Pessoa, *J. Inorg. Biochem*. 2015, **147**, 134-146

61 K. Dhahagani, S. Mathan Kumar, G. Chakkaravarthi, K. Anitha, J. Rajesh, A. Ramu and G. Rajagopal, *Spectrochim. Acta A*, 2014, **117**, 87-94

62. O.J. D'Cruz and F.M. Uckun, *Expert Opin. Invest. Drugs*, 2001, **11(12)**, 1829-1836.

63. G. Sheldrick, SHELXS, *Program for the Solution of Crystal Structure*, 1997.

64. a) H. Hadadzadeh, M. Salimi, M. Weil, Z. Jannesari, F. Darabi, K. Abdi, A. Dehno Khalaji, S. Sardari and R. Ahangari, *J. Mol. Struct*, 2012, **1022**, 172-180; b) V. C. da Silveira, H. Benezra, J. Silva Luz, R. Castro Georg, C. C. Oliveira and A. M. da Costa Ferreir, *J. Inorg. Biochem*., 2011, **105**, 1692-1703.

65. M. Ganeshpandian, R. Loganathan, S. Ramakrishnan, A. Riyasdeen, M. A. Akbarsha and M. Palaniandavar, *Polyhedron*, 2013, **52**, 924-938.

66. J. Toneatto and G. A. Argüello, *J. Inorg. Biochem.*, 2011, **105**, 645-651.

67. G. M. Morris, R. Huey, W. Lindstrom, M. F. Sanner, R. K. Belew, D. S. Goodsell and A. J. Olson, *J. Comput. Chem.*, 2009, **30**, 2785-2791.

68. R. A. Laskowski and M. B. Swindells, *J. Chem. Inf. Model.*, 2011, **51**, 2778-2786.

Figure Captions:

Fig. 1. ORTEP drawing of $[VO(L)_2]$ with the atom numbering. Thermal ellipsoids are shown at the 30% probability level.

Fig. 2. Electronic absorption spectra for the titration of 5.8×10^{-4} M salmon sperm DNA in 20 mM PBS (pH 7.4) with increasing amounts of $[VO(L)_2]$ (6.0×10^{-4} M and 1.2×10^{-3} M, respectively)**.** Appropriate blank samples containing the corresponding concentrations of DNA and the complex were used.

Fig. 3. Electronic absorption spectra for the titration of 4.5×10^{-5} M $[VO(L)_2]$ in 20 mM PBS (pH 7.4) with increasing amounts of salmon sperm DNA**.** Appropriate blank samples containing the corresponding concentrations of DNA and the complex were used.

Fig. 4. (A) Fluorescence spectra of EB-DNA adduct in the absence and presence of increasing amounts of $[VO(L)_2]$. The inset shows plot of F_0/F versus the concentration of $[VO(L)_2]$. (B) Fluorescence spectra of $[VO(L)_2]$, EB in the absence and presence of increasing amounts of $[VO(L)_2]$.

Fig. 5. Cyclic voltammograms of DNA and $[VO(L)_2]$ in the absence and presence of salmon sperm DNA.

Fig.6. Electronic absorption spectra of 2×10^{-5} M BSA in the absence and presence of $[VO(L)_2]$. Appropriate blank samples containing the corresponding concentrations of DNA and the complex were used.

Fig. 7. Fluorescence emission spectra of BSA in the absence and presence of increasing amounts of $[VO(L)_2]$ at (a) 291, (b) 298 and (c) 305 K.

Fig. 8. Plots of log $[(F_0 \ F)/F]$ versus log [Q] for $[VO(L)_2]$-BSA interaction at different temperatures.

Fig. 9. A molecular docking perspective of $[VO(L)_2]$ with DNA using Discovery Studio 4.1 (left) and two-dimensional interactions generated by LIGPLOT+ (right). Groove binding of the complex with partial intercalation into the DNA is observed. Chain A: 5'(C11, G22, C33, G44, A55, A66, T77, T88, C99, G110, C11, G112) 3' and chain B: 3' (G224, C223, G222, C221, T220, T119, A118, A117, G116, C115, G114, C113) 5'

Fig. 10. The docked V(IV) complex in the binding pocket of BSA using Discovery Studio 4.1 (left) and two-dimensional interactions generated by LIGPLOT+ (right).

Fig. 11. The effect of $[VO(L)_2]$ and HL in the concentration range of 0.31-40 μM on the viability of HPG-2 , HT-29 and MCF-7 cell lines. Data are expressed as mean±SEM; n=6 well for each group; * $p<0.05$, ** $P<0.01$ and *** $p < 0.001$ versus control (non-treated) cells; + $p<0.05$, ++ $P<0.01$ and +++ $p < 0.001$ versus [HL]-treated cells in the same doses.

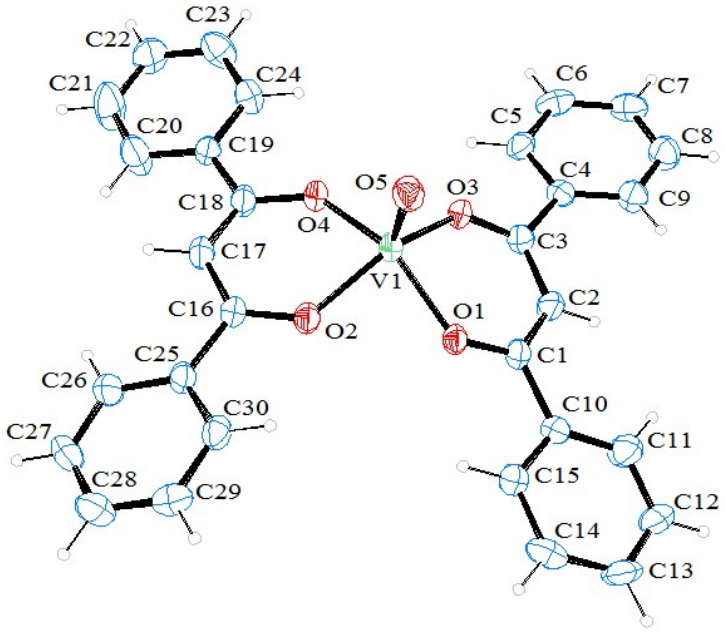

Fig. 1.

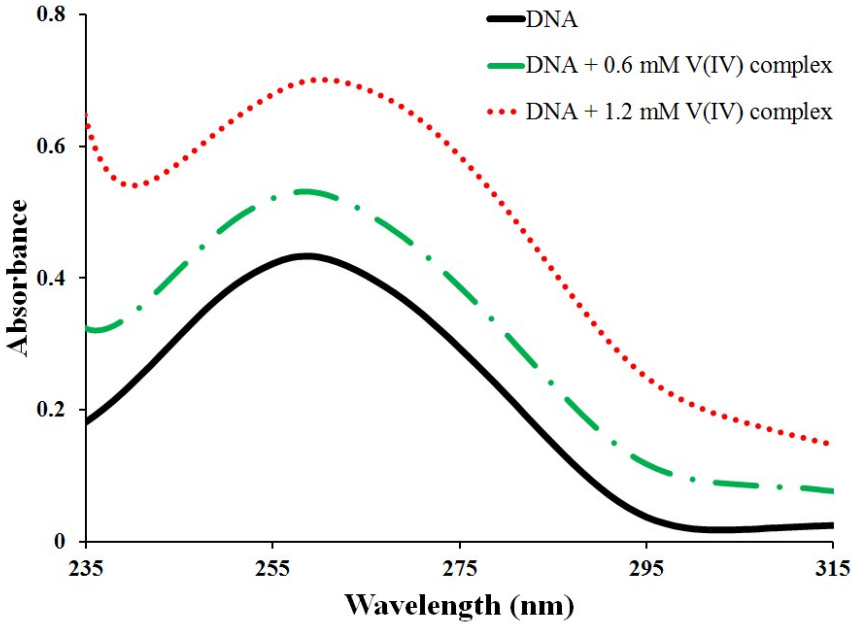

Fig. 2.

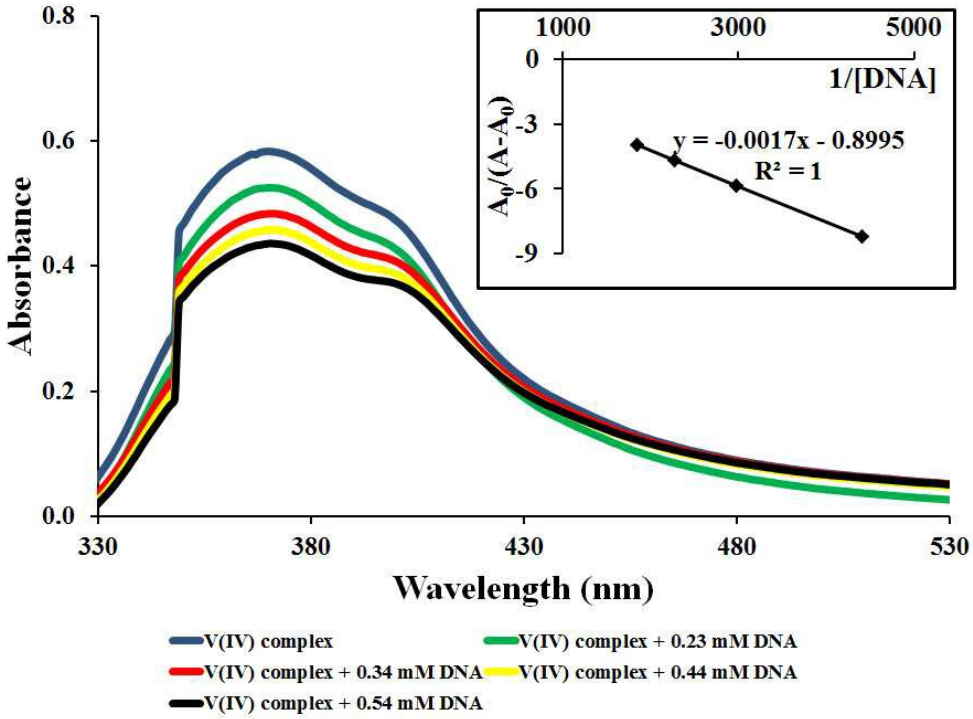

Fig 3.

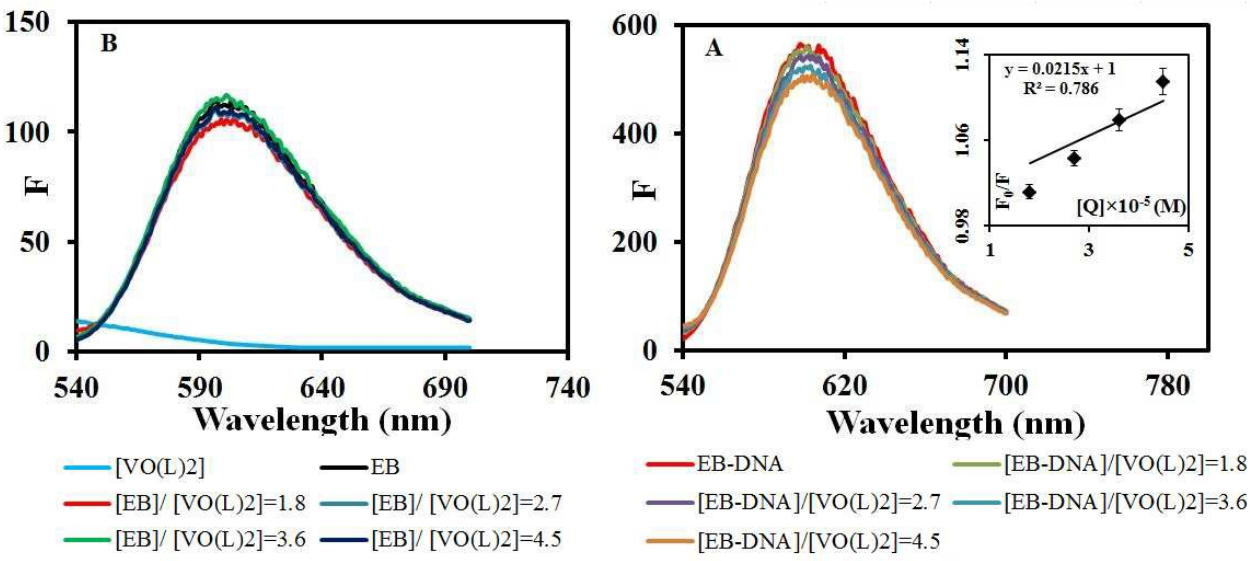

Fig. 4.

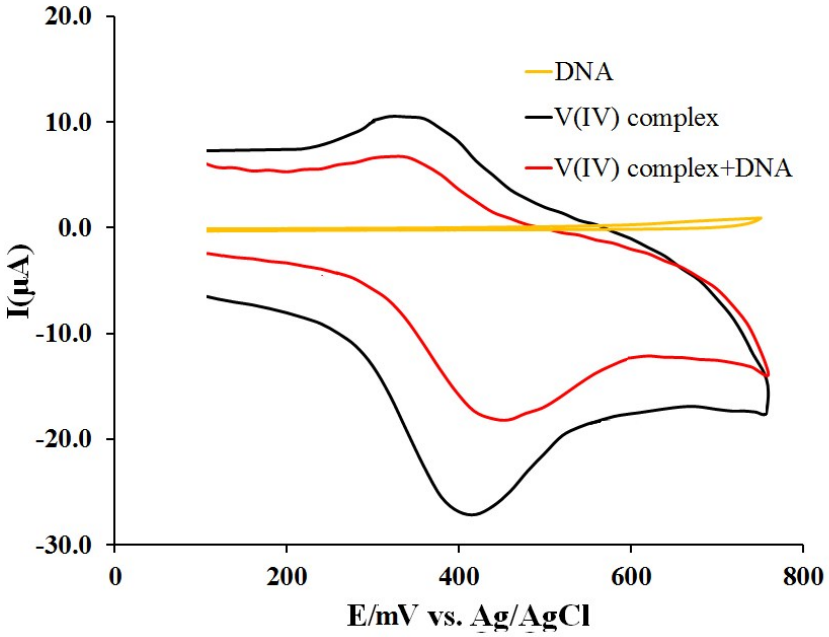

Fig. 5.

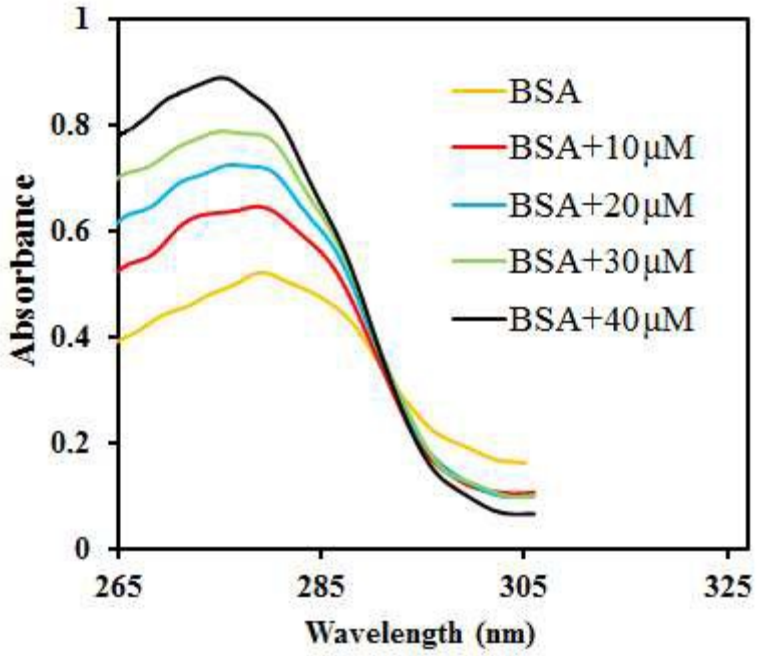

Fig.6.

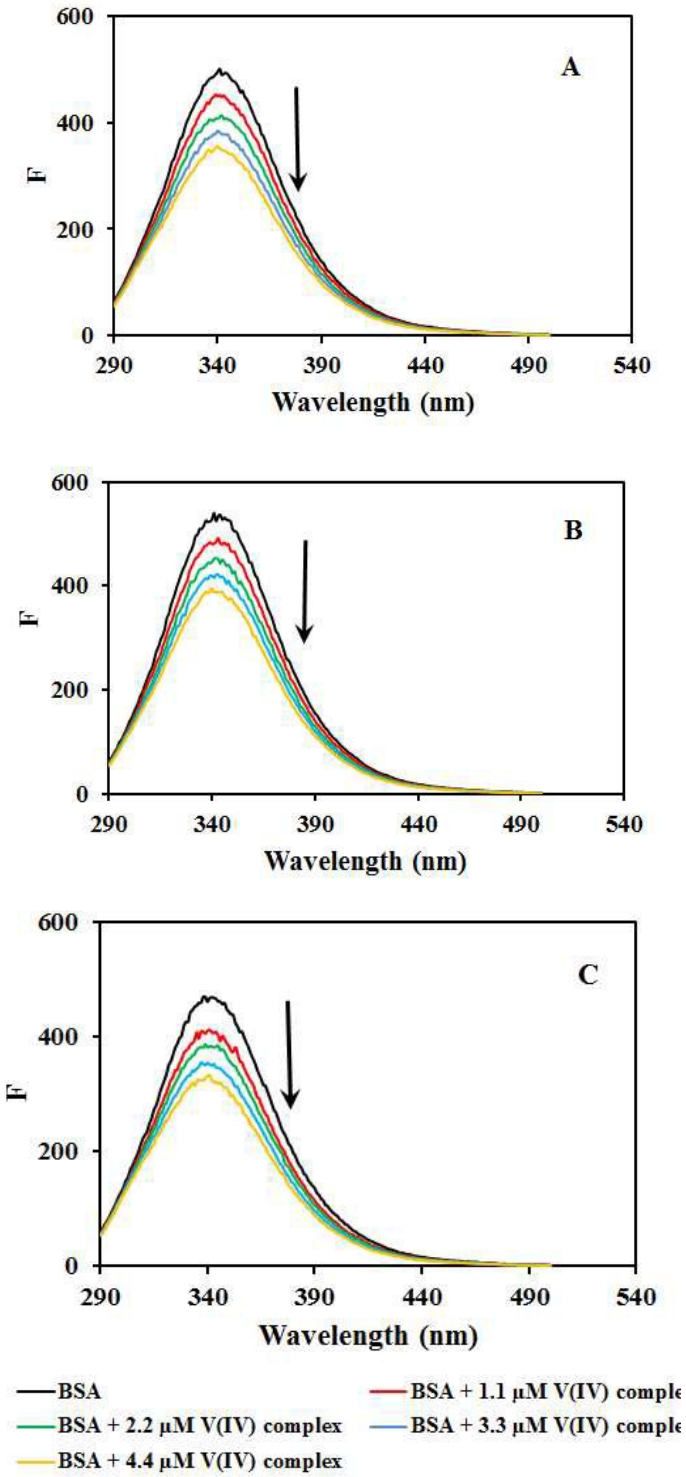

Fig.7

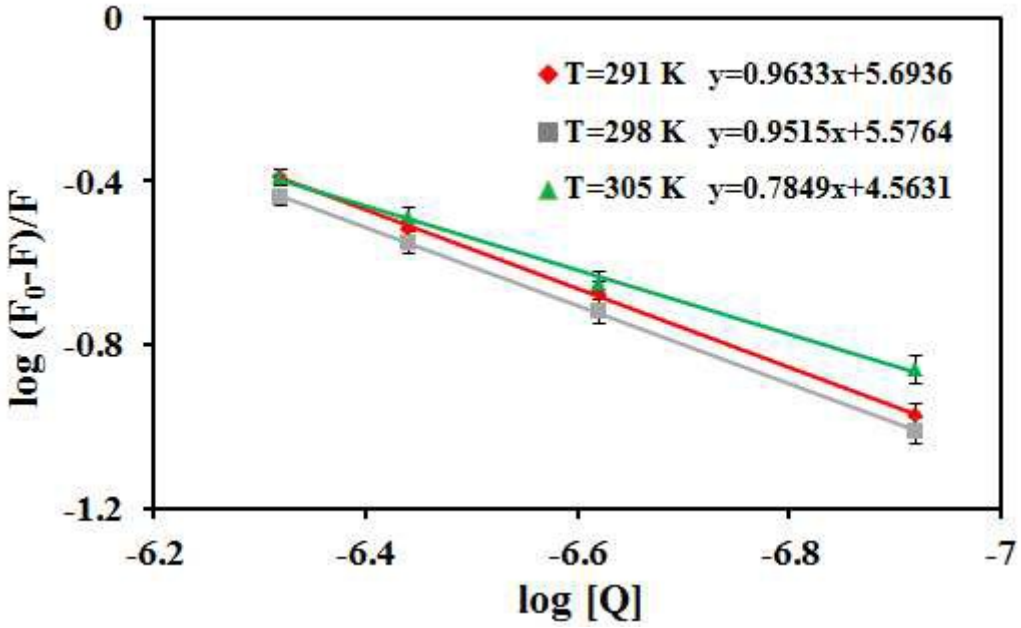

Fig. 8.

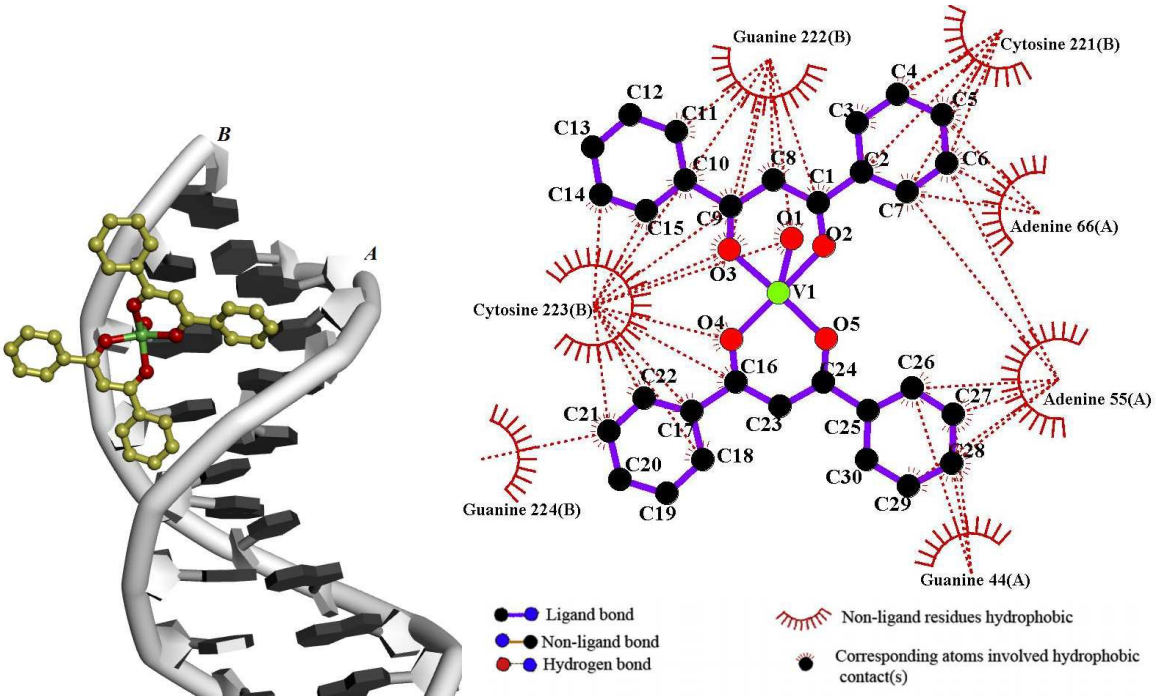

Fig. 9.

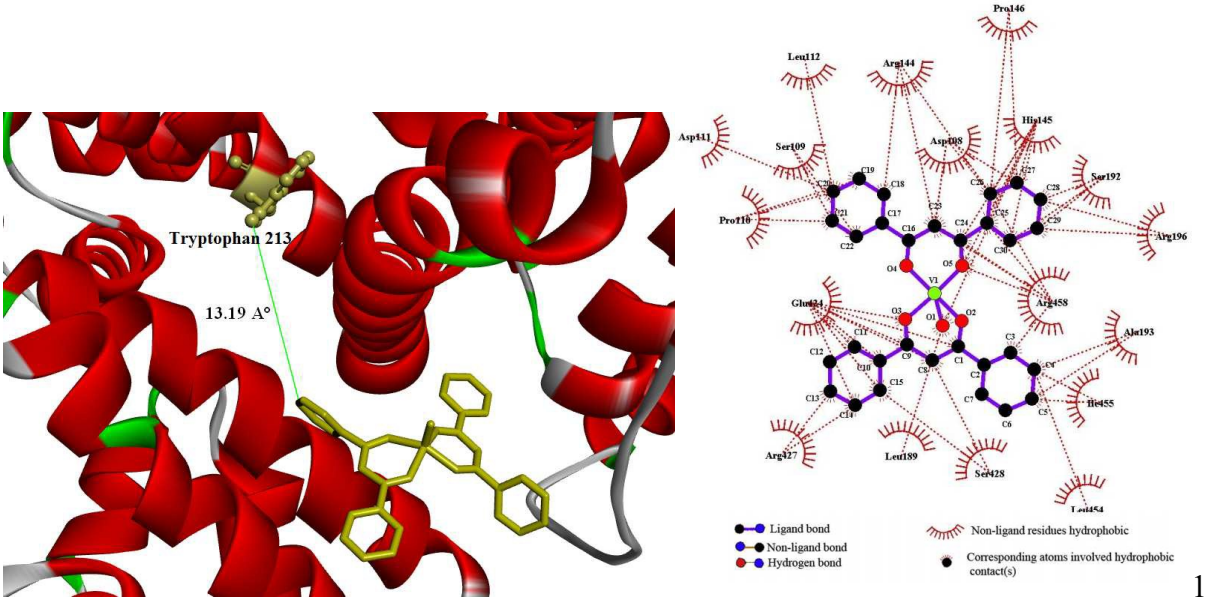

Fig 10.

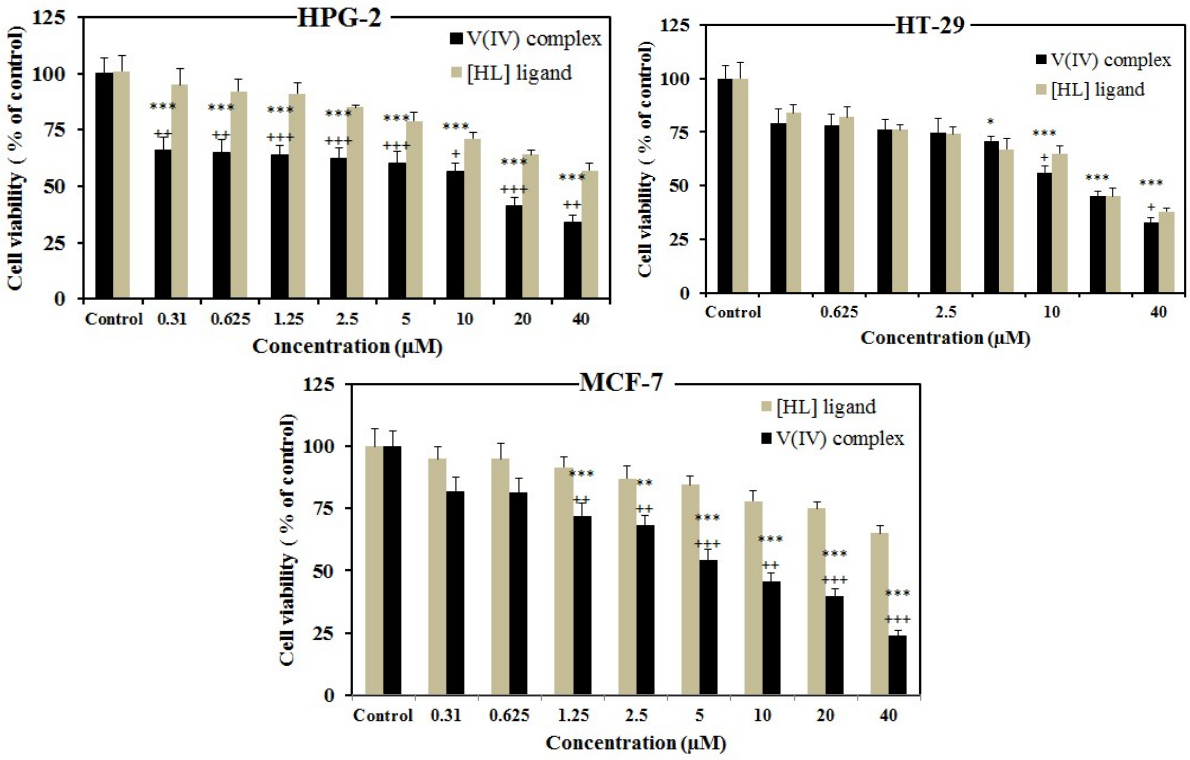

Fig. 11.

Table 1. Bond lengths [Å] and angles [°] for $[VO(L)_2]$.

C(1)-O(1)	1.270(7)	O(1)-V(1)	1.956(4)
C(3)-O(3)	1.257(7)	O(2)-V(1)	1.960(4)
C(16)-O(2)	1.296(7)	O(3)-V(1)	1.969(4)
C(18)-O(4)	1.297(7)	O(4)-V(1)	1.961(4)
O(5)-V(1)	1.579(4)		
C(1)-O(1)-V(1)	130.8(4)	O(1)-V(1)-O(2)	83.72(16)
C(16)-O(2)-V(1)	130.0(4)	O(5)-V(1)-O(4)	107.8(2)
C(3)-O(3)-V(1)	130.9(4)	O(1)-V(1)-O(4)	144.59(18)
C(18)-O(4)-V(1)	130.8(4)	O(2)-V(1)-O(4)	86.66(16)
O(5)-V(1)-O(1)	107.6(2)	O(5)-V(1)-O(3)	105.9(2)
O(5)-V(1)-O(2)	106.2(2)	O(1)-V(1)-O(3)	86.78(16)
O(2)-V(1)-O(3)	147.90(18)	O(4)-V(1)-O(3)	83.54(17)

Table 2. Quenching parameters and binding parameters of the complex-BSA interaction at different temperatures.

T (K)	K_{SV} (10^4 M^{-1})	K_q (10^{12} M^{-1} s^{-1})	$R^{2\,a}$	K_b (10^5 M^{-1})	n	R^2
291	8.41	8.41	0.9996	4.9	0.96	0.9991
298	7.78	7.78	0.9984	3.8	0.95	0.9999
305	8.78	8.78	0.9684	0.37	0.79	0.9967

[a] R^2 is correlation coefficient

Table 3. Thermodynamic parameters of the complex-BSA system at three different temperatures.

T (K)	ΔG (kJ mol^{-1})	ΔH (kJ mol^{-1})	ΔS (J mol^{-1} K^{-1})	R^2
291	-31.6			
298	-29.2	-132.4	-345.4	0.9802
305	-26.8			

Table 4. Crystal data and structure refinement for $[VO(L)_2]$

Empirical formula	$C_{30}\ H_{22}\ O_5\ V$
Formula weight	513.42
Temperature	293(2) K
Wavelength	0.71073 Å
Crystal system	monoclinic
Space group	*P 21/n*
Unit cell dimensions	a = 12.7159(9) Å
	b = 15.199(1) Å
	c = 12.9016(9) Å
	$\alpha = \gamma$ =90º
	β = 96.743(4)
Volume	2476.2(3) $Å^3$
Z	4
Density (calculated)	1.377 Mg/m^3
Absorption coefficient	0.440 mm^{-1}
F(000)	1060
Crystal size	0.18 x 0.08 x 0.06 mm
Theta range for data collection	3.12 to 25.19°.
Index ranges	-14≤h≤15
	-17≤k≤18
	-15≤l≤15
Reflections collected / unique	9435 / 4443 [R(int) = 0.0591]
Data Completeness	0.997
Absorption correction	Semi-empirical from equivalents
Max. and min. transmission	0.9741 and 0.9251
Refinement method	Full-matrix least-squares on F^2
Data / restraints / parameters	4443 / 19 / 325
Goodness-of-fit on F^2	1.049
Final R indices [I>2σ(I)]	R_1 = 0.0857
	wR_2 = 0.1951
R indices (all data)	R_1 = 0.1894
	wR_2 = 0.2386
Largest diff. peak and hole	0.547 and -0.247 e.$Å^{-3}$

A mononuclear diketone-based oxido-vanadium(IV) complex: structure, DNA and BSA binding, molecular docking and anticancer activities against MCF - 7, HPG-2, and HT- 29 cell lines

Maryam Mohamadi, S.Yousef Ebrahimipour *, Masoud Torkzadeh-Mahani, Sabine Foro, Alireza Akbari